

Characterization of Expansion Tube Flows for Hypervelocity Combustion Studies

Adela Ben-Yakar* and Ronald K. Hanson†
Stanford University, California 94305-4085

An expansion tube with an 89 mm inner diameter and a 12 m length was characterized for basic studies of the near-field mixing and flame-holding characteristics of gaseous fuels injected in high-stagnation-enthalpy supersonic flows. The expansion tube provides a wide range of freestream conditions with little perturbation of test gas chemical composition. The latter is critical for supersonic-combustion studies in the high-stagnation-enthalpy flows associated with hypersonic airbreathing propulsion systems. Efforts focused on achieving three operating points, simulating flight Mach 8, 10, and 12 stagnation-enthalpy conditions at the entrance of a supersonic combustor. The ability of the expansion tube to provide a steady-flow test time of adequate duration and a core flow of sufficient size for 2-mm jet-in-crossflow studies was verified. A core-flow size of 25 mm could be achieved in 6.2 MJ/kg stagnation-enthalpy flows with 400 μ s of steady test time (flight Mach 12 simulation). The primary effects of the boundary layer on the expansion tube flow were to extend the useful test time (in contrast with conventional shock-tube performance) and to decrease the core-flow size.

Nomenclature

Da	=	Damköhler number
J	=	jet to freestream momentum flux ratio, $(\gamma p M^2)_j / (\gamma p M^2)_\infty$
L	=	characteristic length
L_1	=	characteristic distance from edge of the injection plate
L_2	=	characteristic recirculation region length
M	=	Mach number
M_s	=	shock Mach number
M_w	=	molecular weight
p	=	static pressure
q	=	dynamic pressure
Re	=	Reynolds number
T	=	static temperature
t	=	time
U	=	velocity
x	=	distance
γ	=	specific heat ratio
γ_c	=	average specific heat ratio, $\frac{1}{2}(\gamma_0 + \gamma_3)$
η_c	=	compression efficiency through a hypersonic vehicle diffuser
θ	=	characteristic temperature for the ignition delay time
v_i	=	gas composition
ρ	=	density
τ_c	=	chemical time
τ_i	=	ignition delay time

Subscripts

j, jet	=	jet properties at the injection exit
0	=	atmosphere conditions
1	=	driven section conditions

Received 1 June 2001; revision received 12 January 2002; accepted for publication 12 February 2002. Copyright © 2002 by Adela Ben-Yakar and Ronald K. Hanson. Published by the American Institute of Aeronautics and Astronautics, Inc., with permission. Copies of this paper may be made for personal or internal use, on condition that the copier pay the \$10.00 per-copy fee to the Copyright Clearance Center, Inc., 222 Rosewood Drive, Danvers, MA 01923; include the code 0748-4658/02 \$10.00 in correspondence with the CCC.

*Postdoctoral Research Fellow, High Temperature Gasdynamics Laboratory, Applied Physics Department, 450 Via Palou; adela@stanford.edu. Student Member AIAA.

†Professor, High Temperature Gasdynamics Laboratory, Mechanical Engineering Department, Building 520. Fellow AIAA.

3	=	supersonic combustor entry conditions
4	=	driver section conditions
10	=	expansion section conditions
∞	=	freestream

Introduction

THE success of future hypersonic airbreathing propulsion systems will be largely dependent on efficient injection, mixing, and combustion processes inside the supersonic/hypersonic combustion chamber. The combustor entry conditions (Mach number, static temperature, and pressure) of this type of engine depend on the flight conditions of the vehicle. For flights beyond Mach 6, flow should remain supersonic throughout the engine to avoid excessive performance losses due to the normal shock wave system and to avoid chemical energy losses due to dissociation.

Studies of supersonic combustion are performed mainly in two flight regimes: at flight speeds of Mach 8 and below^{1–5} and at flight speeds higher than Mach 8 (Refs. 6–22). Because of the large stagnation enthalpies (greater than 3 MJ/kg) associated with high flight Mach numbers beyond Mach 8, currently only impulse facilities are capable of providing the required stagnation temperature and Mach number to replicate a combustor environment. Expansion tubes and reflected shock tunnels are two possible types of impulse facilities for ground testing. Of concern for high-stagnation-enthalpy simulations is the chemical composition of the test gas. In reflected shock tunnels, the test gas is contained at stagnation conditions, and significant amounts of dissociated species are formed. Dissociation in expansion tubes, on the other hand, may be negligible.¹⁷ Therefore, an expansion tube can provide a more representative simulation of the true flight combustion chemistry including ignition delay and reaction times. In general, however, expansion tubes have shorter test times than reflected shock tunnels. The principal advantages and disadvantages of expansion tubes as compared to other hypersonic test facilities, especially shock tunnels, are summarized in Table 1.

Examples of existing impulse-type facilities include 1) the free-piston reflected shock tunnel, T5, located at the Guggenheim Aeronautical Laboratory, California Institute of Technology¹¹; 2) Calspan reflected shock tunnel⁹; and 3) the expansion tube HYPULSE located at the General Applied Science Laboratories.^{6–8} In these facilities, generic combustor models with hydrogen injection have been tested using conventional measurement techniques such as pressure measurements along the combustor and flow visualization with differential interferometry. However, only limited number of data has been collected because of the long preparation times of each single experiment in these large facilities.

Table 1 Advantages and disadvantages of expansion tubes relative to shock tunnels for hypervelocity combustion simulations

Shock tunnels	Expansion tubes
Significant level of radicals such as O and NO are produced in the test gas above flight Mach 10 affecting the combustion chemistry. In the reflected zone of the shock tube, air dissociates due to high temperatures and recombines only partially during the fast expansion process.	Negligible amount of radicals is produced when simulating below about flight Mach 16. The working gas never stagnates, thus reduces the extent of dissociation. As a result, the test gas reaches to the test section with more accurate chemical composition.
The facility needs to contain the stagnation pressures and temperatures of the flow it generates. As noted by Anderson, ¹⁵ at flight Mach numbers above 12, the stagnation pressure requirements approaches 10 ⁶ psi or 68,000 atm, which can be produced only by expansion tubes.	Higher stagnation pressures and temperatures can be achieved in the expansion tubes even for the same initial driver pressure and sound speed, as velocity is added to the flow through the unsteady expansion process without stagnating it.
Freestream Mach number is fixed by the nozzle geometry. Simulation of different conditions requires replacement of the nozzle with a new geometry or throat size.	Variable Mach numbers and conditions can easily but not independently be obtained by just altering the initial filling pressures.
Nozzle can be damaged due to the high heat transfer rates at the throat and flying diagrams inside the tube.	High heat transfer rates are avoided in the absence of a sonic throat. However, the test object is prone to damage from flying diagrams arriving at the end of the expansion tube operation.
Boundary layer develops throughout the nozzle and can be thick compared to the dimensions of the injection port. It is usually required to eliminate the boundary layer by, for example, inserting a step before the fuel injection port. ⁴	A thin boundary layer is developed upstream of the injection port as the injection plate is placed in the freejet exiting the tube.
Test times ≈ 1 ms. However, a substantial part of it is wasted during the nozzle startup time (of the order of 0.5 ms) required for the supersonic flow to be established. Test time decreases with increasing stagnation enthalpy.	Test times $\approx 0.2 - 0.5$ ms. No nozzle startup time is required. In addition, the establishment of flow on the studied model begins during the expansion section gas flow before the test gas arrival. As a result, less useful test time is consumed during the flow establishment.
Test section is longer because of the longer test time and larger core flow. However, side wall effects should be taken into account.	Test section dimensions depend on the size of the core flow at the exit of the tube, which is diminished by the boundary-layer growth on the tube walls.

In the present study, a small-size expansion tube is used to generate stagnation-enthalpy conditions in the Mach 8–12 flight range. This allows to generate a relatively accurate supersonic burner entry condition, namely, a radical-free, high-stagnation-enthalpy airflow. These unique properties of flow conditions are important in fundamental studies of the mixing, ignition, and flame-holding mechanisms of different injection concepts. The small size of the facility enables more frequent experiments, up to 10 per day, an advantage compared to larger impulse-type facilities that can average a limited number of experiments per day.

This paper presents the efforts made in characterizing the expansion tube test flow to replicate three nominal combustion entry conditions for flight Mach 8, 10, and 12. First, the paper presents a discussion on the issues related to flight simulation: the flow conditions that are expected at the entrance of a supersonic combustor, the critical flow parameters to be considered in flight simulation, and the experimental approach taken in the current study including the facility itself and the measurement techniques. Second, the characterization of the test flow is presented. Several issues such as the useful test time, core-flow size, and boundary-layer effects are addressed to characterize fully the flow generated in the expansion tube.

Flight Simulation Discussion

Typical Supersonic Burner Entry Conditions

There are several issues important in the design of flow parameters of a supersonic propulsion system. The flight Mach number M_0 should increase as the altitude of the vehicle increases. This is required to keep the density inside the combustor high for efficient combustion and the lift at reasonably high values. Residence time is another issue that has to be considered for efficient performance of a high-speed propulsion system. The air must be compressed in the diffuser to reduce velocities and increase the flow residence time and, therefore, allow a combustor of reasonable length. On the other

hand, the reduced velocities at the combustor entry are restricted by the maximum allowable compression temperature T_3 in the range of 1440–1670 K (Ref. 23) to avoid excessive dissociation in the exhaust flow.

The theoretical values of flow conditions at the combustor entrance of an airbreathing propulsion system can be estimated considering the aforementioned issues. Figure 1 shows theoretical values of burner entry Mach number M_3 , pressure p_3 , and the corresponding flight height as a function of flight Mach number M_0 .

Figure 1a shows the theoretical burner entry Mach number for different burner entry temperature to atmosphere temperature ratios T_3/T_0 . When adiabatic compression (constant stagnation enthalpy) is assumed throughout the inlet, the temperature ratio can be written as

$$\frac{T_3}{T_0} = \frac{1 + [(\gamma_0 - 1)/2]M_0^2}{1 + [(\gamma_3 - 1)/2]M_3^2} \quad (1)$$

As shown in Fig. 1a, for hypersonic flights beyond Mach 6 ($M_0 > 6$), a supersonic combustion ramjet (scramjet), where the flow remains supersonic/hypersonic throughout the engine, should be considered.

Figure 1b shows theoretical values for burner entry pressure p_3 . To keep structural loads on the hypersonic vehicle at acceptable levels the dynamic pressure, $q_0 = (\frac{1}{2})\rho_0 U_0^2$, must be kept in the range of 50–100 kPa. Consequently, flight at high speeds is confined to altitudes of 25–40 km. When these fixed dynamic pressure values are considered, and compression efficiency $\eta_c = 0.9$ and temperature ratio $T_3/T_0 = 6$ are assumed, the burner entry pressure can be estimated using the following equation¹:

$$\frac{p_3}{p_0} = \left(\frac{T_3/T_0}{T_3/T_0(1 - \eta_c) + \eta_c} \right)^{\gamma_c/(\gamma_c - 1)} \quad (2)$$

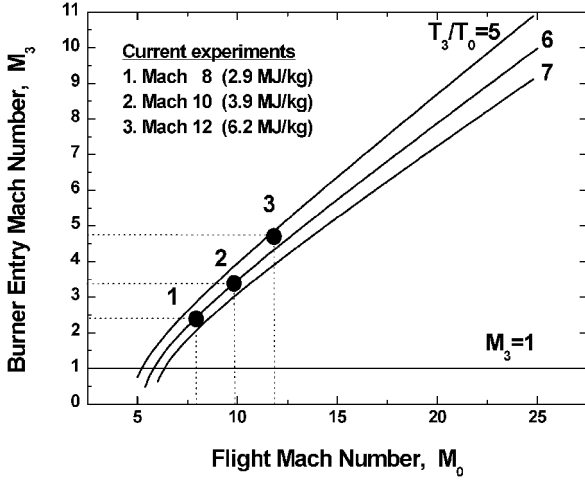
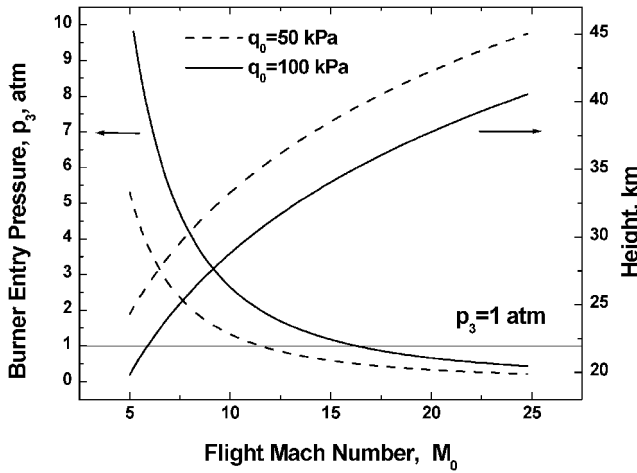
a) Burner entry Mach number M_3 b) Burner entry pressure p_3 and the flight height

Fig. 1 Theoretical scramjet burner entry conditions as a function of flight Mach number, calculated assuming adiabatic compression and air with constant specific heat ratio of $\gamma_c = \frac{1}{2}(\gamma_0 + \gamma_3) = 1.36$.

In these calculations, air is assumed a calorically perfect gas having constant specific heat ratio of $\gamma_c = \frac{1}{2}(\gamma_0 + \gamma_3) = 1.36$. Typical pressures at the entrance of supersonic combustors range from approximately 0.2 to 4 atm depending on the operating parameters for the flight mission, such as the Mach number and the dynamic pressure.

Critical Parameters in Supersonic Combustion Simulation

An experimental simulation of a supersonic reacting flow requires the replication of five parameters^{14,15}: pressure p , temperature T , velocity U , characteristic length of the model L , and gas composition v_i . These simulation parameters can be manipulated to provide the flight values of generalized nondimensional flow parameters such as the following.

Mach number:

$$M \sim U / \sqrt{T} \quad (3)$$

Reynolds number:

$$Re \sim \rho U L / \sqrt{T} \sim \rho L (U / T^{\frac{1}{2}}) \quad (4)$$

Damköhler number:

$$Da \sim L / U \tau_c \quad (5)$$

Damköhler number represents the ratio of flow residence time through the combustor, L/U , to chemical time τ_c and must be

larger than one to achieve flame holding and a complete combustion process. For flame-holding considerations, ignition delay time τ_i replaces the chemical time τ_c in Damköhler number expression. For a hydrogen-air combustion process, the ignition delay time τ_i varies inversely with pressure because of the two-body reactions. Additionally, τ_i depends exponentially on temperature. As a result, Damköhler number can be related to basic flow parameters:

$$Da \sim pL / [U \cdot \exp(\theta/T)] \quad (6)$$

where θ is a characteristic temperature for the ignition time.

Preservation of the values of these three nondimensional parameters can be achieved through proper simulation of all five basic parameters. However, note that if the flow chemical composition, flow velocity, and temperature are duplicated, then a constant value of the product pL would satisfy the requirements for simulation of the three nondimensional parameters. Therefore, from the standpoint of mixing and flame-holding studies, a correct simulation of only four parameters seems essential: chemical composition, temperature, velocity, and the product pL .

Experimental Approach

In the current experiments, three of the four parameters discussed earlier are duplicated: the flow chemical composition v_i , the required burner entry velocity U_3 , and burner entry static temperature T_3 . The fourth flow parameter, the freestream static pressure p_3 is, however, below that of actual systems. Furthermore, because the characteristic length scale in the experiments is small, about 2 mm (the diameter of the fuel injection orifice), the parameter pL is not sufficiently high to replicate a real combustor environment. This will result in chemical kinetic limitations on the H_2 -air ignition and combustion processes. On the other hand, this limitation can partially be circumvented if an elevated concentration of oxygen is used in the test gas to increase the collision rates as suggested by Bakos et al.⁷ However, Ben-Yakar²² has shown that, in high-enthalpy flows, presented in this paper, ignition of hydrogen, injected transversely into a freestream of air, can be achieved in the near vicinity of the injector, even at low pL values. If ignition is achieved at low pressures, it is, therefore, likely that autoignition will occur at higher pressures because the Damköhler and Reynolds numbers increase linearly with pL in a realistic system.

In conclusion, the most important parameters that have to be replicated for fundamental supersonic combustion studies are chemical composition, temperature, and velocity of the freestream. A less important parameter is the product pL . Variation in pressure affects the ignition time linearly, whereas variation in temperature has an exponential effect through the activation energy (and, hence, the characteristic temperature θ) in chemical kinetics.

An ultimate objective of this research is to investigate near-field mixing and flame-holding characteristics of different gaseous fuels, such as hydrogen and ethylene, injected transversely from a single orifice into a realistic supersonic combustor environment. The use of an expansion tube provides a wide range of variability in the freestream conditions with relatively accurate chemical composition.

Table 2 summarizes the three nominal test flow conditions, Mach 8, Mach 10, and Mach 12, achieved using the Stanford expansion tube facility. The use of this facility enables acceleration of the air to stagnation-enthalpy conditions (3–6 MJ/kg_{air}) corresponding to the Mach 8–12 flight range, without exposing it to high stagnation temperatures (3000–6000 K). Therefore, the freestream contains negligible amounts of radicals, produced only by the incident shock wave. During the expansion tube operation, the test gas is first shocked to its maximum temperature (1700–2150 K) and then accelerated and cooled to the required static temperature (1250–1400 K). Through this unsteady expansion process, the stagnation temperature and pressure of the gas increase.

Expansion Tube Facility

The Stanford expansion tube facility is schematically shown in Fig. 2. The tube is 12 m in length (including dump tank) with an inner

Table 2 Test gas (freestream) flow properties simulating the burner entry conditions of three flight Mach numbers, corresponding values from Fig. 1

Flight simulation	Mach 8	Mach 10	Mach 12
<i>Initial filling pressures</i>			
Driven section, He, psig (MPa)	300 (2.17)	600 (4.24)	600 (4.24)
Driven section, 95%N ₂ + 5%CO ₂ , psia (kPa)	0.45 (3.10)	0.5 (3.45)	0.15 (1.04)
Expansion section, He, torr (kPa)	70 (9.31)	20 (2.67)	2 (0.27)
<i>Freestream conditions</i>			
Stagnation enthalpy, MJ/kg	2.9 ± 0.05	3.9 ± 0.1	6.2 ± 0.15
Mach number	2.40 ± 0.03	3.38 ± 0.04	4.66 ± 0.07
Static temperature, K	1400	1290	1250
Static pressure, atm (kPa)	0.65 (65.9)	0.32 (32.4)	0.04 (4)
Velocity (measured), m/s	1800 ± 20	2360 ± 25	3200 ± 50
Test time (measured), μs	170 ± 10	270 ± 10	400 ± 10
Test slug length (velocity × test time), m	0.31	0.64	1.28
Establishment length for laminar boundary layer at L ₁ = 50 mm, m	0.15	0.15	0.15
Maximum measured recirculation region length, L ₂ , d _{jet} = 2 mm	~1.5d _{jet}	~2d _{jet}	~4d _{jet}
Establishment time for the jet upstream recirculation region based on (30–70) × L ₂ , m	0.09–0.21	0.12–0.28	0.24–0.56
Freestream Reynolds number at the injection port, Re _x = 50 mm	2.9 × 10 ⁵	2.2 × 10 ⁵	3.8 × 10 ⁴
Boundary-layer thickness upstream of the injection port, mm	0.65	0.75	1.80
Shock speeds in the expansion section (measured), m/s	2468	3175	3650
Shock Mach number in the expansion section	2.44	3.14	3.61
Maximum temperature that the test gas is exposed to, T ₂ , K	1690	1750	2140

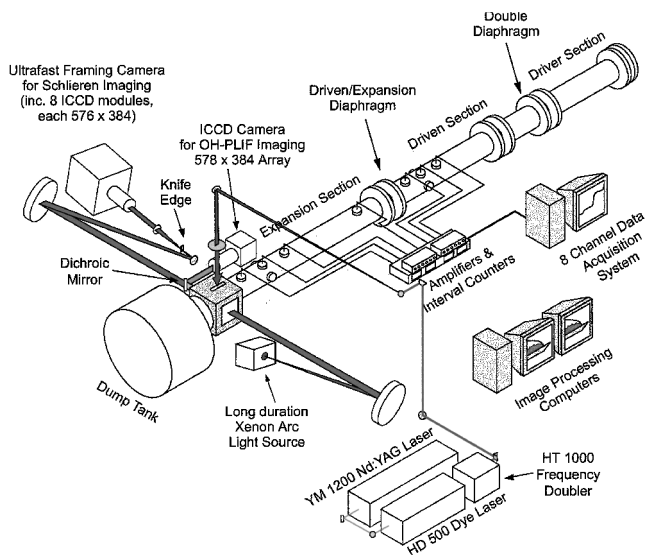


Fig. 2 Expansion tube facility (12 m in length and 89 mm inner diameter) and imaging system.

diameter of 89 mm and includes driver, driven, and expansion sections. The driver section is filled with high-pressure helium gas and is separated by double diaphragms from the lower pressure driven section, which is filled with the desired test gas. Mylar® film (6.35 μm thick) is used as the diaphragm material at the driven/expansion interface to separate the test gas from low-pressure helium gas of the expansion section. Also shown in Fig. 2 are the optical diagnostic devices, including lasers and optical arrangement for planar

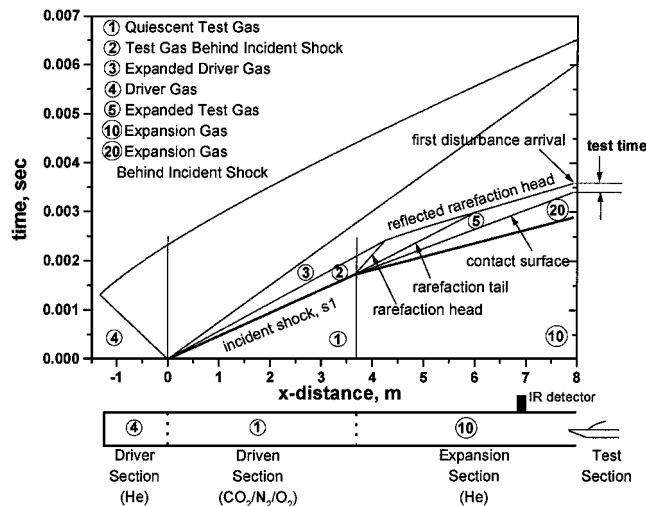


Fig. 3 Expansion tube distance-time (x-t) diagram calculated for flight Mach 12 condition; method of characteristics used to solve the flow gasdynamics properties.

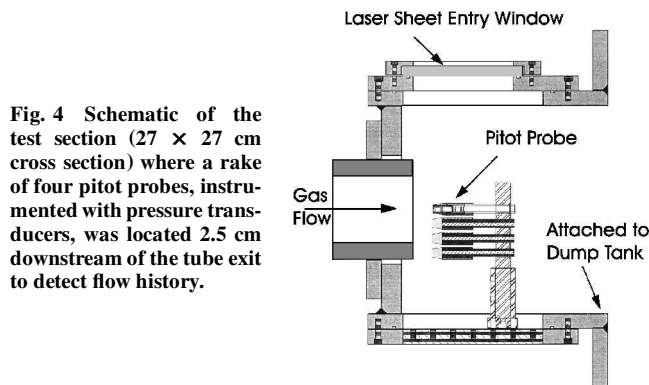


Fig. 4 Schematic of the test section (27 × 27 cm cross section) where a rake of four pitot probes, instrumented with pressure transducers, was located 2.5 cm downstream of the tube exit to detect flow history.

laser-induced fluorescence imaging, and a megahertz framing-rate intensified digital camera for schlieren imaging.

The operating sequence of an expansion tube is best represented by the distance-time (x-t) diagram. Figure 3 is an example of an x-t diagram calculated for the Mach 12 flight condition. The method of characteristics was used to solve the flow gasdynamics properties assuming one-dimensional inviscid theory. Test time is defined as the time that the test gas has uniform flow quantities and is determined by the arrival time of the contact surface to the tube exit and that of the first subsequent rarefaction wave (reflected rarefaction head in our case of high total enthalpy simulations).

The double diaphragms are ruptured, generating a shock wave that propagates into the test gas. The shocked test gas is then accelerated by an unsteady and constant area expansion process from the driven section into the lower pressure expansion section. This unsteady expansion process adds kinetic energy that increases stagnation temperature and pressure without stagnating the gas. The test gas emerging from the downstream end of the expansion, thus, has both a higher stagnation enthalpy and higher effective stagnation pressure than the shock tube flow from which it originated. Further detail on the operating cycle of an expansion tube can be found in the review papers of Erdos⁸ and Anderson.¹⁵

A square test section of 27 × 27 cm cross section is mounted at the exit of the expansion tube. This section is equipped with an opposed pair of square (13 × 13 cm) quartz windows and a fused silica slot on top of the chamber for admission of the vertical laser sheet (as shown in Fig. 4).

Six piezoelectric pressure transducers are mounted along the driven and expansion sections for shock speed and wall pressure measurements. An additional transducer, mounted 20.3 cm downstream of the driven/expansion interface, is used to monitor the unsteady expansion process.

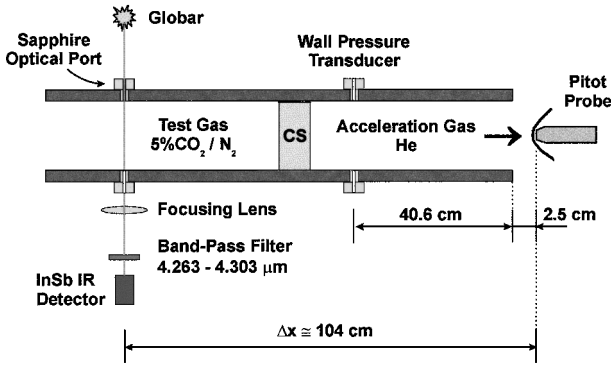


Fig. 5 IR emission setup to measure the test gas velocity, which is assumed equal to the CS velocity.

The expansion section is equipped with sapphire viewing ports for optical measurements. An InSb infrared (IR) detector (Judson J-10 InSb equipped by a Perry Model 720 amplifier) is mounted at the sapphire viewing port located 101.6 cm from the end of the tube (Fig. 5). The arrival of the test gas is detected through the emission of IR light from 5% CO₂ seeded into the nitrogen test gas. In addition, for flow characterization tests, a pitot rake consisting of four pressure transducers across the diameter of the tube is positioned at the test section, 2.5 cm downstream of the tube exit (Fig. 4). The test gas velocity can then be calculated by considering its time of arrival at the viewing port and at the pitot rake, which are positioned $\Delta x = 104$ cm apart from each other. Data from these sensors are recorded at 1 megasamples/s on an eight-channel (12-bit) computer scope.

Test Flow Characterization Results

Several issues were addressed to characterize fully the properties of the supersonic flow generated in the expansion tube facility. Of particular concern were the determination and characterization of flow conditions, the steady-flow test time, the core-flow size, and the boundary-layer effects on the flow properties.

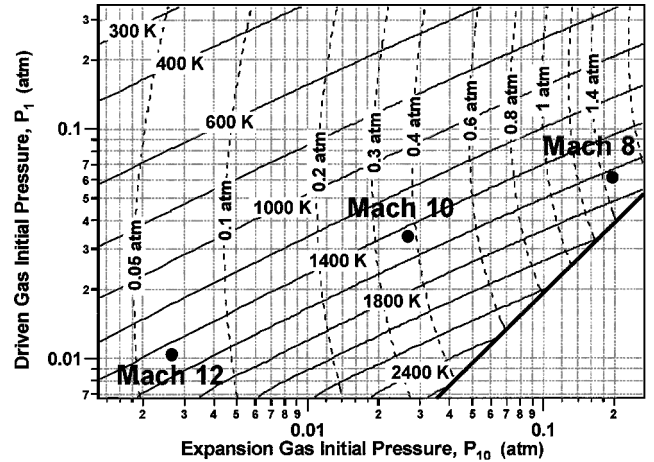
Flow Conditions

Flow conditions at the exit of an expansion tube depend on the initial filling pressures and the sound speed of the gases in the different sections of the expansion tube. In this facility, helium gas was used in the driver section with a maximum filling pressure of 42 atm (600 psig). In the expansion section, low-pressure helium was used (see Table 2).

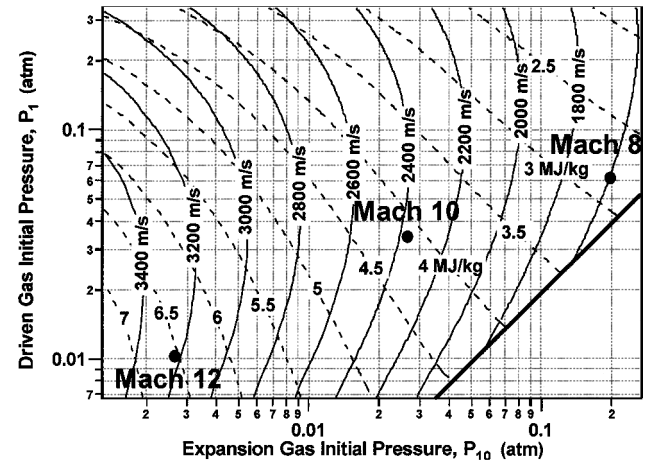
The initial pressures required to achieve the desired flow conditions have been calculated using a simple one-dimensional inviscid theory for a driver (helium) filling pressure of 42 atm (600 psig). Results of the calculations are presented as maps in Fig. 6. Note that the effective filling pressure of the driver section is taken as $P_{4, \text{eff}} = 54.5$ atm (788 psig) because its inner diameter (10.16 cm) is larger than that of the driven and expansion sections (8.89 cm). This area difference is accounted for in the curves presented in Fig. 6. These maps provide guidelines in the selection of the initial pressures for different conditions of interest.

The heavy solid lines in the lower right of Figs. 6a and 6b mark the boundary where the pressure of shocked test gas, p_2 , is less than in the expansion section, p_{10} . However, in theory, the pressure p_2 should always be larger than p_{10} because the main purpose of an expansion tube is stagnation-enthalpy multiplication through the unsteady expansion process.

In a conventional shock tube, for a given driver initial pressure, one must decrease the driven section pressure to generate flows with higher velocities, temperatures, and Mach numbers. As the driven section initial filling pressure decreases, the shock-induced static pressure decreases as well. In expansion tubes, on the other hand, the flow velocity and its static pressure do not vary significantly as the driven initial pressure is changed for a given driver and expansion section pressure. As shown in Fig. 6, different velocities can be



a) Pressure and temperature



b) Stagnation enthalpy and velocity of the test gas

Fig. 6 Maps of estimated test flow (nitrogen) conditions (state 5) at the exit of an expansion tube with different initial driven and expansion section pressures.

achieved by manipulating the expansion section initial pressure. For lower expansion section pressures, the flow accelerates to higher velocities and expands to lower pressures.

In the experiments, the maps in Fig. 6 were used to determine the initial pressures to simulate the required burner entry conditions of flight Mach 8, 10, and 12. Simulation of Mach 10 flight condition, for example, corresponds to 4 MJ/kg of stagnation enthalpy and a Mach number of about 3.5. Therefore, in accordance with the maps in Fig. 6, initial filling pressures of the expansion and driven sections were determined to be 20 torr and 0.50 psia, respectively, to simulate flight Mach 10 stagnation enthalpy condition at the selected driver initial pressure of 600 psig. Initial pressures required to simulate flight Mach 8 and 12 were chosen in a similar manner and are marked on the maps of Fig. 6.

As discussed in the preceding section, the experimental approach includes correct replication of the velocity and temperature of the air entering the combustor. The static pressure in our experiments, on the other hand, is lower than the expected values in a supersonic combustor at those flight conditions. However, the correct replication of pressure is not as crucial as the simulation of the required stagnation temperature and burner entry Mach number, in the basic study of ignition and flame-holding processes of different injection schemes. Pressure dependence of the ignition process can be extrapolated to higher pressures because the Damköhler number is approximately proportional to pressure in hydrogen-air combustion systems. Furthermore, the oxygen concentration can be increased in the test gas if the combustion process is rate limited due to low static pressure.

Table 2 summarizes the initial filling pressures of the three test conditions characterized in the Stanford expansion tube. Other factors, such as the maximum available injector pressure, were taken into account in determining these test flow conditions. The initial driver pressure for the Mach 8 condition, for example, was chosen to be 300 psig instead of 600 psig to provide reasonable penetration of the fuel jet. Penetration of fuels injected transversely into supersonic flows is known to be strongly correlated with the jet-to-freestream momentum flux ratio J defined as

$$J = \frac{(\rho u^2)_j}{(\rho u^2)_\infty} = \frac{(\gamma p M^2)_j}{(\gamma p M^2)_\infty} \quad (7)$$

where the subscript j corresponds to the jet exit conditions and ∞ corresponds to freestream conditions ahead of a bow shock. In our experiments, the jet-to-freestream momentum flux ratio was typically $J = 1.5$ – 2 .

Measurement of Flow Properties

The test flow conditions (pressure, temperature, velocity, Mach number, and test time), presented in Table 2, were determined using the combined data of wall static pressure, pitot pressure (stagnation pressure behind a normal shock wave), and IR emission. Briefly, the test flow characterization was performed in the following stages.

1) The shock speeds at the driven and expansion sections were measured using six piezoelectric pressure transducers mounted in the tube.

2) Gasdynamic conditions of the postshock test gas in the driven and expansion sections were obtained from the measured shock speeds by a one-dimensional frozen-chemistry code using standard thermochemical data.

3) The test gas temperature and sound speed at the exit of the tube were then calculated assuming isentropic expansion of the shocked test gas in the driven section to the theoretical value of the postshock static pressure of the acceleration gas in the expansion section. The degree of dissociation is low at all phases of the thermodynamic cycle in the expansion tube; thus, the test gas can be assumed in equilibrium during the unsteady expansion (an isentropic process.)

4) The velocity of the contact surface was deduced by measuring the time interval between its arrival at the IR detector port and the pitot probe located at the exit of the tube.

5) Test gas flow velocity was then estimated by equating the contact surface velocity with that of the test gas immediately after it.

An example of IR emission from CO_2 seeded in the test gas, together with pitot and static pressure traces measured in flight Mach 10 flow simulation, is given in Fig. 7. In Fig. 7, $t = 0$ is incident shock arrival at the pitot probe, placed 2.5 cm downstream of the tube exit, whereas the wall pressure transducer and IR detector are positioned 40.6 and 101.6 cm upstream of the tube exit, respectively (Fig. 5). Note that the timescale of the static pressure trace is shifted by 235 μs to match the shock arrival at the pitot probe. In characterization experiments, instead of air, a 5% CO_2 seeded into N_2 was used as a test gas to detect the test gas arrival from CO_2 IR emission. This 95% $\text{N}_2 + 5\% \text{CO}_2$ mixture also provides an effective molecular weight ($M_w = 28.8$ g/mole) equivalent to that value of the air. Based on the pitot pressure history at the tube exit, it is possible to identify the arrival of the shock wave, the period of expansion section helium flow, the helium/test gas contact surface, and the steady flow test time. It is evident that the contact surface is not a perfectly sharp boundary between helium and test gas. Instead, test gas concentration seems to increase over a period of time.

Similar trends can be observed in IR emission, which can be detected with the arrival of the helium/test gas contact surface (CS) to the viewing port. The intensity of IR emission increases through the CS passage as the CO_2 concentration in the CS increases. At the end of the steady test gas, the emission intensity decreases as the test gas cools down with the arrival of the expansion waves (reflected rarefaction tail). During the steady flow test time, we observe that the IR emission is not as constant as the traces of the pitot and static pressures. Instead, an initial peak followed by a monotonic increase is observed in the Mach 10 flow characterization (Fig. 7).

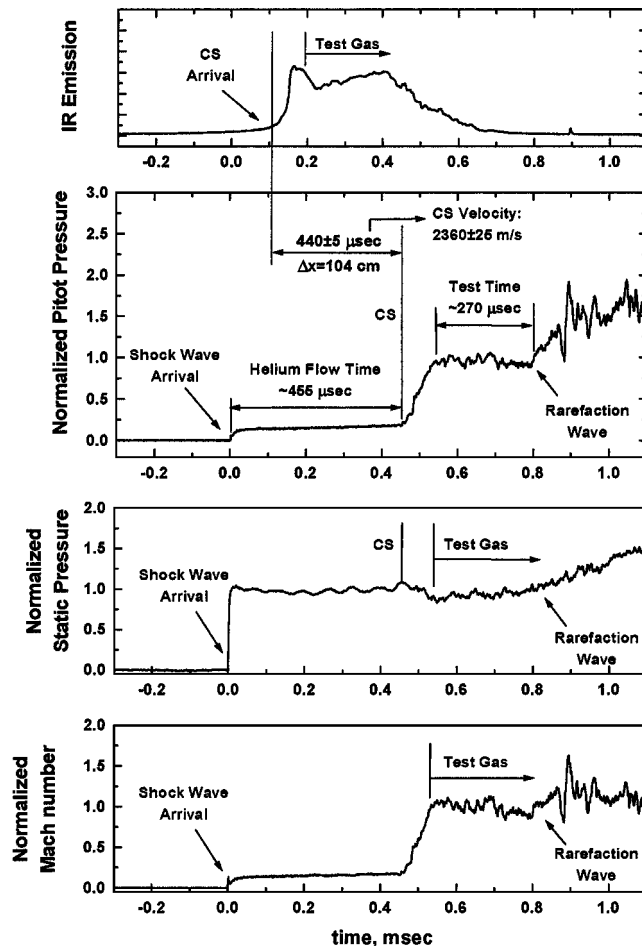


Fig. 7 Example of IR emission, pitot pressure, wall pressure records, and Mach number variation based on the pitot-to-static pressure ratios, as a function of time for the Mach 10 flow condition.

In general, the intensity of IR emission increases with the volume of emitting gas, its temperature, and concentration. Because the IR emission is the integrated emission across the tube including the wall boundary layer, it does not reflect the properties of the core flow only. The monotonic increase of the intensity (subsequent to the drop from its initial peak value) can be explained as due to an increase in the volume of the hotter CO_2 in the growing boundary layer, whereas the initial peak signal can be attributed to the small hot region formed by the reflected shock during the break of the helium/test gas diaphragm.

The steady test period was taken to be the time over which the pitot pressure was changed by no more than $\pm 5\%$ from the average value. Accordingly, the measured test time was approximately 270 μs . The steady test period is always limited by the arrival of waves, either the unsteady expansion waves (rarefaction tail) or the reflected waves (reflected rarefaction head) from the intersection of the driver gas interface with the unsteady expansion waves. In any case, the arrival of waves is clearly identifiable as the test gas pressure rises sharply and the IR emission from cooling test gas begins to decrease.

An average value of 2360 m/s for the test gas flow velocity was measured over the 104 cm length between the IR emission port and pitot rake (see stages 4 and 5 described earlier). The test gas velocity was also estimated from measured shock speeds in the expansion section using inviscid one-dimensional theory, resulting in 2130 m/s. The measured velocity (2360 m/s), therefore, exceeds the estimated inviscid value based on shock speed by approximately 10%. The increase in measured velocity can be explained by the acceleration of the flow due to the growing boundary layer on the tube walls.

The Mach number of the test gas was calculated using the measured contact surface velocity and calculated sound speed as described in stage 3. The results indicated an exit Mach number of

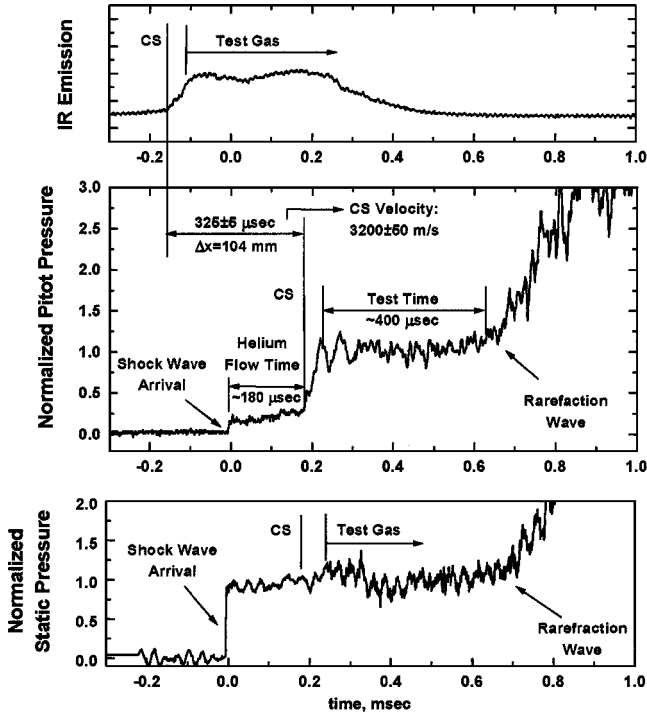


Fig. 8 Example of IR emission, normalized pitot pressure, and normalized wall static pressure traces as a function of time for Mach 12 flow condition.

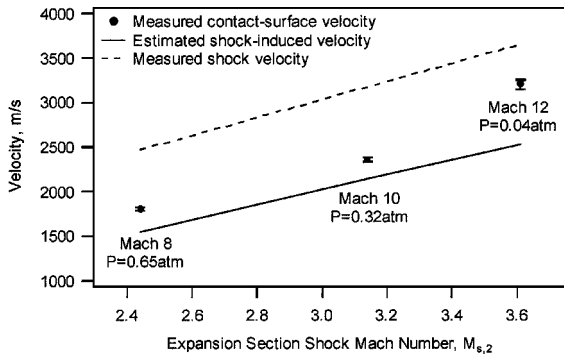


Fig. 9 Comparison of the measured CS velocity (test gas velocity) with the shock-induced gas velocity estimated using measured shock speeds in the expansion section.

3.38 ± 0.04 in the Mach 10 flight condition. Mach number variation during the test gas can also be obtained from the pitot to static pressure ratio as shown in Fig. 7. Note that although the static pressure of the test gas rose sharply after the arrival of the reflected rarefaction wave, the Mach number of the flow varied little over the following 400–500 μ s.

Figure 8 shows an example of flight Mach 12 flow characterization traces, which have features similar to those of flight Mach 10 traces. The characterization results show a relatively long test time of 400 μ s in the case of flight Mach 12 simulation; this is much larger than the ideal values (180 μ s). The test gas velocity was measured to be 3200 m/s, about 23% faster than the shock-induced ideal flow velocity. This acceleration of the test gas is again believed to be a result of the boundary layer developed on the tube walls.

Comparison of the measured values of the freestream velocity with the expected values estimated using the measured shock speeds in the expansion section are shown in Fig. 9. The results indicate that the measured velocities are always larger than the expected ideal values. In addition, as the flight Mach number increases and, therefore, the static pressure decreases, the measured gas velocity approaches the shock velocity. These observations suggest that boundary-layer effects are significant, causing the flow to be nonuniform. Because

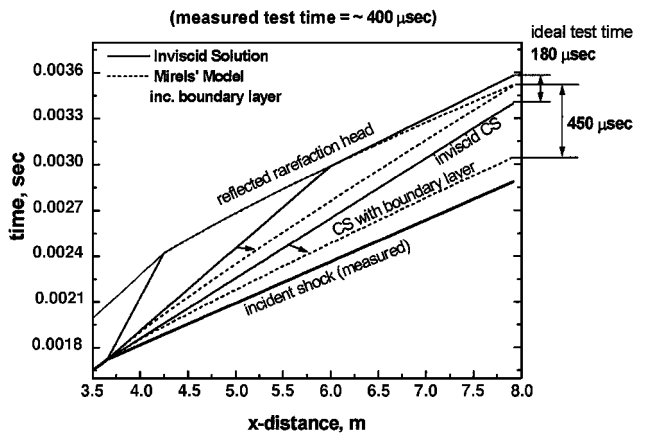
of viscous effects, the shock slows down, and the contact surface (test gas) accelerates. At the limit of a sufficiently long expansion section, boundary-layer effects would cause the shock and the contact surface to equilibrate to a constant velocity. Accordingly, an additional calculation, taking into account the viscous effects based on Mirels’s solution^{24,25} for postshock boundary layers has been performed and will be discussed in the following section.

Boundary-Layer Effects on Test Time

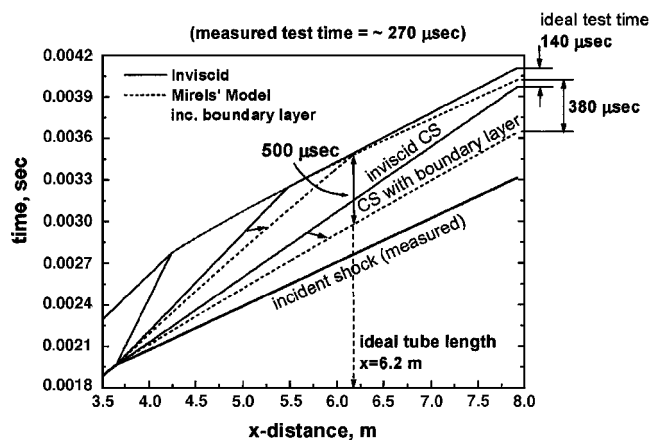
The uniform flow time of test gas at the expansion tube exit is defined as the test time; this period begins with the arrival of the driven/expansion contact surface at the tube exit and ends with arrival of the first rarefaction wave (in our case, the rarefaction head reflected from driver/driven contact surface as shown in $x-t$ diagram in Figs. 3 and 9).

Under ideal conditions, where no wall effects exist, the shock wave and the contact surface would move with constant velocities, and the flow between them would be uniform. However, in a real shock tube, the flow becomes nonuniform as the boundary layer develops at the tube walls. The presence of a wall boundary layer causes the incident shock to decelerate and the contact surface to accelerate. Consequently, the time duration of the flow between the shock and the contact surface (expansion section helium flow time) is reduced. In conventional shock tubes, therefore, the test time is reduced because of the boundary-layer growth.

In expansion tubes, on the other hand, the effect of the boundary layer in accelerating the contact surface can actually lead to an increase in test time as observed in the experiments. At the Mach 12 condition, 400 μ s of steady test time was measured, whereas the expected value was only 180 μ s based on one-dimensional inviscid calculations. (See the $x-t$ diagram in Fig. 10a.)



a) Mach 12 condition



b) Mach 10 condition

Fig. 10 Expansion section only, $x-t$ diagrams: straight lines one-dimensional inviscid calculations and dashed lines results from applying Mirels’s model^{24,25} to include the boundary-layer effects.

Table 3 Summary of measured, ideal (inviscid, one dimensional) and predicted (based on Mirels's solution^{24,25}) properties of test gas for Mach 10 and 12 flow conditions

Based on	Test time, μ s	Test gas velocity, m/s	Helium flow time, μ s
<i>Mach 10</i>			
Measured	270 \pm 10	2360 \pm 25	455 \pm 2
Ideal	140	2130	660
Mirels's solution	380	2510	520
<i>Mach 12</i>			
Measured	400 \pm 10	3200 \pm 50	180 \pm 2
Ideal	180	2440	520
Mirels's solution	450	3300	170

To study the boundary-layer effects on the test time, an improved calculation was performed taking into account the viscous effects based on Mirels's boundary layer solution.^{24,25} The variation of contact surface velocity was calculated using Mirels's model by using the measured value of the incident shock velocity and assuming it constant along the expansion section. This more realistic contact surface velocity was, then, implemented in $x-t$ diagram calculations, and the results are plotted together with one-dimensional inviscid calculations in Fig. 10a. The calculations, including boundary-layer effects (dashed lines in Fig. 10a), resulted in test time of 450 μ s, agreeing well with the measured value of 400 μ s. This effect can be explained by that the contact surface, accelerated by viscous effects, arrives at the test section earlier than if viscous effects were negligible. Therefore, the test time duration is increased as the time arrival of the first flow disturbance is delayed relative to the contact surface arrival.

An additional interesting result can be observed from the $x-t$ diagrams: The length of the current expansion section is seen to be optimum to achieve a maximum test time duration for Mach 12 flight simulation. The arrival of both the rarefaction wave and the reflected rarefaction head overlap at the end of the tube (see the dashed lines in Fig. 10a). Any variation in the length of the expansion section will cause the test time to decrease. As shown in the $x-t$ diagrams, the reflected rarefaction head travels faster (shallower angle in the $x-t$ diagram: $1/V = t/x$) than both the rarefaction tail and the contact surface. Therefore, the test time is the longest when the rarefaction tail overlaps with the reflected rarefaction head. The $x-t$ diagram calculated for the Mach 10 condition (Fig. 10b) demonstrates that the expansion section length is, however, longer than its optimum value. A 30% longer test time could have been achieved if the expansion section was 1.8 m shorter than its current length. (Test time at $x = 6.2$ m is about 500 μ s, see Fig. 10b.) Beyond the 6.2 m length of the expansion section, the test time shortens with distance because the reflected rarefaction head (the first test flow disturbance) travels faster than the contact surface.

The calculation based on Mirels's solution^{24,25} also gives an improved estimation of the expansion section helium flow time of 170 μ s, which compares well with that inferred from the pitot pressure trace, 180 μ s (within 5.5% accuracy). The test gas velocity obtained from this calculation, 3300 m/s, shows improved agreement with the measured value of 3200 (within 3%). These results, summarized in Table 3, confirm the importance of boundary-layer effects and demonstrates that the viscous calculations based on Mirels's model provide good estimates of the test time and the test gas velocity at the low-pressure Mach 12 flight condition.

Mirels's solution,^{24,25} performed for the Mach 10 flight condition (Fig. 10b), results in a less accurate prediction of flow properties. As summarized in Table 3, the calculated test time based on Mirels's solution overpredicts (by 41%) the actual test time. The reason for the overprediction is that the initial filling pressure in the expansion section is relatively high (20 torr), and therefore, the wall boundary layer behind the shock wave is not fully developed as assumed in Mirels's solution. In addition, it was assumed that the boundary-layer properties of the test gas were similar to the properties of the expansion section helium gas, which can be significantly different as the pressure increases.

It has been shown that the flow test time is affected by the boundary-layer development in the expansion section tube walls in such a way that the steady test time duration is increased. Longer test times are important in supersonic flow experiments because the length of the test period determines the maximum model length in which steady flow can be fully established.

Core-Flow Size

The other parameter that limits the maximum model length is the radius of the axially uniform flow called the useful core flow. Although the test time increases as the boundary layer on the tube walls develops, the useful core-flow size becomes smaller. The thickness of the boundary layer developed in the acceleration section can be large in comparison to the tube radius because of the low filling pressures of the expansion section.

In the experiments, the useful core-flow size was characterized by measuring the pitot pressure at different radial and axial locations. The results, plotted in Fig. 11, show that at 12.7 mm (0.5 in.) away from the tube exit, pitot pressure varied only $\pm 5\%$ within a 25 mm core-flow diameter for the three conditions studied. As the pitot probe was moved downstream of the tube exit, the core-flow size at the Mach 12 condition did not change significantly. On the other hand, the Mach 10 and 8 flight conditions resulted in a decreased core-flow size away from the tube exit. At the Mach 8 condition, pitot pressure at the centerline of the tube decreased by 15% at

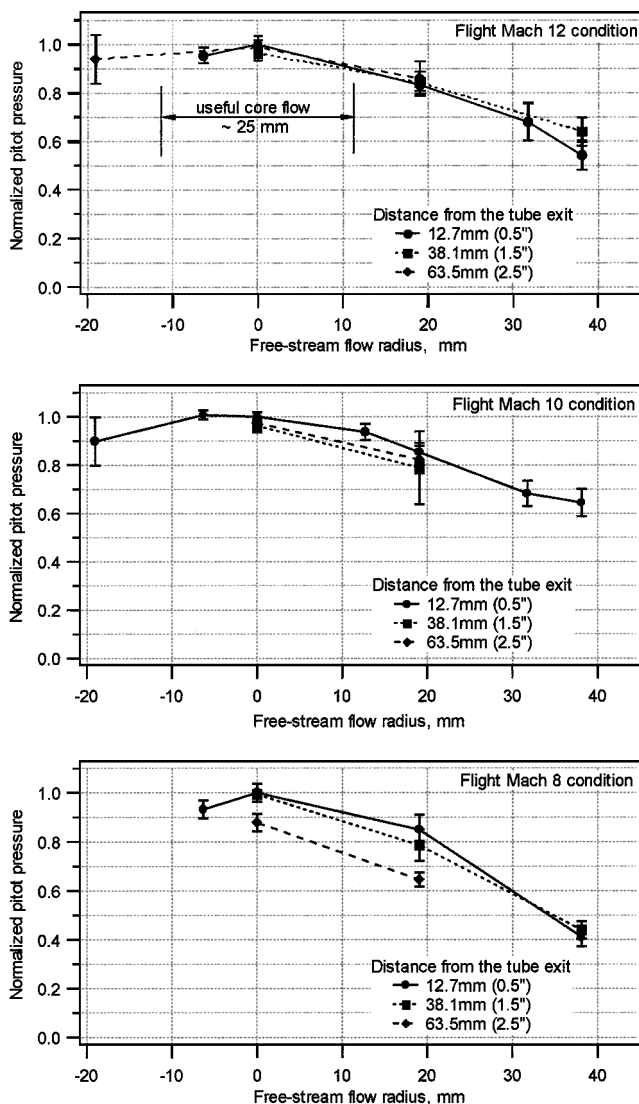


Fig. 11 Useful core-flow size in different flight conditions determined by measuring the radial variation of pitot pressure at different distances from the tube exit.

63.5 mm (2.5 in.) downstream of the tube exit. This result was expected for the Mach 8 flight condition because the Mach number of the freestream is only about 2.4, corresponding to a steeper Mach wave angle.

In conclusion, the results indicate the existence of a 25-mm core flow that is suitable for near-field studies of transverse fuel jets injected from a 2-mm-diam orifice. The injection plate is positioned as close as possible to the tube exit and 6.4 mm ($\frac{1}{4}$ in.) below the centerline to allow a maximum field of study of the jet.

Flow Establishment Time

Part of the steady test time is consumed during the flow establishment process for the model under investigation. Correlations are available in the literature^{26–29} for predicting the flow establishment times for different flow features of the model. In general, the test “slug length,” defined as the distance traveled by the volume of test gas during the period of steady test time, must be larger than the characteristic length of the flow device or process by some multiple. The criterion for the establishment of flow over a flat plate requires that the test slug length, that is the product of test time and gas velocity, $t \cdot U$, satisfies²⁸

$$t \cdot U \geq \begin{cases} 2 \cdot L_1 & \text{for turbulent boundary layer} \\ 3 \cdot L_1 & \text{for laminar boundary layer} \end{cases} \quad (8)$$

where L_1 is the distance from the edge of the plate. The flow establishment criterion for separated flows, on the other hand, is required to be tens of times larger than the characteristic recirculation region length L_2 , as given by Holden²⁹ for the wake of sphere

$$t \cdot U \geq \begin{cases} 30 \cdot L_2 & \text{based on pressure measurements} \\ 70 \cdot L_2 & \text{based on heat transfer measurements} \end{cases} \quad (9)$$

Note that L_2 is the length of the recirculation region and, therefore, smaller than the characteristic distance L_1 by more than an order of magnitude, resulting in similar flow establishment times.

Based on these correlations, two flow establishment times in the experiments were estimated and summarized in Table 2. First, the boundary-layer flow establishment time was calculated by assuming laminar flow because the local Reynolds numbers at the injection port were relatively small. Second, the establishment time of the recirculation region upstream of the injection port was estimated. In general, the bow shock around the jet interacts with the approaching boundary layer and causes its separation. This recirculation region length confined with the separation shock wave was measured from schlieren images and used as the characteristic length L_2 of the separation zone.

The estimated flow establishment values indicated that the test slug (1.28 m) for the Mach 12 flight condition is fairly long compared to the predicted flow establishment times (0.15 m for boundary layer and 0.56 m for the recirculation region heat transfer establishment time is equal to 0.71 m in stagnation). Therefore, about 0.60 m of a test slug or 235 μ s of a test time is still available for measurements. By contrast, at the flight Mach 8 condition, flow establishment seems to consume most of the steady test time. However, note that the expansion section helium flow before to the test gas arrival contributes to the establishment of jet flow even though it is not considered as a part of the test time. Furthermore, the useful test time in the experiments is determined using the pitot probe after the flow is established around it. Therefore, the estimated flow establishment times given in Table 2 are expected to be larger than the actual flow establishment times, so that, even at the flight Mach 8 condition, part of the slug length is useful for measurements after the flow field is established.

To summarize, as the flight Mach number in the facility increases, a longer test slug length becomes available for measurements. This is a result of the long test times achieved with high-stagnation-enthalpy, low-pressure conditions and because higher speed implies faster flow establishment.

Conclusions

This paper summarized the feasibility of using an expansion tube to generate clean (radical-free), high-stagnation-enthalpy supersonic flows of air associated with hypervelocity combustors. Characterization experiments with test gas mixture of 95%N₂ + 5%CO₂ were performed to study the facility performance such as the freestream flow properties, the useful test time, and the core-flow size available for mixing and combustion studies of a 2 mm jet-in-crossflow.

The experimental approach included simulation of the required stagnation enthalpy (3–6 MJ/kg_{air}) of Mach 8, 10, and 12 flight conditions by simulating the required burner entry Mach number, burner entry static temperature, and consequently the burner entry velocity. Because the burner entry static temperatures were chosen to be in the range of 1250–1400 K, velocities of 1800, 2360, and 3200 m/s were generated for the Mach 8, 10, and 12 flight conditions, respectively. On the other hand, simulated static pressures were below the desired values because of the limited maximum pressures available in the current driver section and the limited maximum pressures at which the jet injector valve could operate sufficiently fast. With the filling pressure of 42 atm in the driver section, static pressures of 1.3, 0.32, and 0.04 atm could be achieved for the Mach 8, 10, and 12 flight conditions, respectively.

The steady test time duration and the core-flow size of the expansion tube flow were characterized. These are important parameters that define the model dimensions where a fully established flow can be achieved. In addition, primary effects of the boundary layer on expansion tube flow were observed. In particular, test times ranging between 170 and 400 μ s, higher than the ideal values, were observed. In contrast with shock tunnels, in the expansion tube, an increased duration of useful test times can be achieved as the corresponding flight Mach number of the test flow increases. The boundary layer developed on the tube walls increases the contact surface velocity and, therefore, delays the arrival of the first disturbance wave. However, note that, in the experiments, the static pressure of the freestream was low for high-enthalpy flows, causing the boundary-layer effects to increase the test time. Simulation with higher pressures might result in shorter test times and, therefore, shorter useful test slug lengths would be available.

It was demonstrated that Mirels’s solution^{24,25} for boundary-layer effect implemented in $x-t$ diagrams is a useful tool for prediction of test time and in optimization of the expansion section length to achieve the maximum test duration.

Pitot pressure surveys at the exit of the expansion tube have identified an inviscid test core of approximately 25 mm diameter over which the pitot pressure is constant to within $\pm 5\%$. Whereas the core-flow size in Mach 10 and 12 conditions did not diminish significantly at 6.35 cm downstream of the tube exit, the core-flow size for the Mach 8 condition dropped by half. Because the Mach wave angle is steeper for small freestream Mach numbers, the boundary-layer information at the tube exit reaches to the centerline in a smaller distance at the Mach 8 flight condition.

Finally, compared to large facilities that can average a limited number of experiments per day, in this facility many experiments per day can be performed with the effort of only one student. Therefore, this facility provides a useful tool for basic study of near-field features of different fuel injection configurations that have potential for future application in scramjet engines.

Acknowledgments

The work has been supported by the U.S. Army Research Office, with David Mann as Technical Monitor and by the Air Force of Scientific Research, Aerospace and Materials Sciences Directorate, with Julian Tishkoff as Technical Monitor. The authors gratefully acknowledge the contributions of M. Kamel and C. Morris to this investigation.

References

- Allen, M. G., Parker, T. E., Reinecke, W. G., Legner, H. H., Foutter, R. R., Rawlins, W. T., and Davis, S. J., “Fluorescence Imaging of OH and

NO in a Model Supersonic Combustor," *AIAA Journal*, Vol. 31, No. 3, 1993, pp. 505-512.

²McMillin, B. K., Seitzman, J. M., and Hanson, R. K., "Comparison of NO and OH Planar Fluorescence Temperature Measurements in Scramjet Model Flowfields," *AIAA Journal*, Vol. 32, No. 10, 1994, pp. 1945-1952.

³Gruber, M. R., Nejad, A. S., Chen, T. H., and Dutton, J. C., "Mixing and Penetration Studies of Sonic Jets in a Mach 2 Freestream," *Journal of Propulsion and Power*, Vol. 11, No. 2, 1995, pp. 315-323.

⁴Parker, T. E., Allen, M. G., Foutter, R. R., Sonnenfroh, D. M., and Rawlins, W. T., "Measurements of OH and H₂O for Reacting Flow in a Supersonic Combusting Ramjet Combustor," *Journal of Propulsion and Power*, Vol. 11, No. 6, 1995, pp. 1154-1161.

⁵Santiago, J. G., and Dutton, J. C., "Velocity Measurements of a Jet Injected into a Supersonic Crossflow," *Journal of Propulsion and Power*, Vol. 13, No. 2, 1997, pp. 264-273.

⁶Bakos, R. J., Tamagno, J., Rizkalla, O., Pulsonetti, M. V., Chinitz, W., and Erdos, J. I., "Hypersonic Mixing and Combustion Studies in the Hypulse Facility," *Journal of Propulsion and Power*, Vol. 8, No. 4, 1992, pp. 900-906.

⁷Bakos, R. J., Tamagno, J., Trucco, R., Rizkalla, O., Chinitz, W., and Erdos, J. I., "Mixing and Combustion Studies Using Discrete Orifice Injection at Hypervelocity Flight Conditions," *Journal of Propulsion and Power*, Vol. 8, No. 6, 1992, pp. 1290-1296.

⁸Erdos, J. I., "Recent Experiments on Hypersonic Combustion in an Expansion Tube Test Facility," *Combustion in High-Speed Flows*, edited by J. D. Buckmaster, T. L. Jackson, and A. Kumar, Kluwer Academic Publisher, 1994, pp. 53-91.

⁹Albrechtinski, T., Boyer, D., Chadwick, K., and Lordi, J., "Calspan's Upgraded 96-Inch Hypersonic Shock Tunnel: Its Development and Application in the Performance of Research and Testing at Higher Enthalpies," AIAA Paper 95-0236, Jan. 1995.

¹⁰Wendt, M. N., and Stalker, R. J., "Transverse and Parallel Injection of Hydrogen with Supersonic Combustion in a Shock Tunnel," *Shock Waves*, Vol. 6, Springer-Verlag, Berlin, 1996, pp. 53-59.

¹¹Bélanger, J., and Hormung, H., "Transverse Jet Mixing and Combustion Experiments in Hypervelocity Flows," *Journal of Propulsion and Power*, Vol. 12, No. 1, 1996, pp. 186-192.

¹²McIntyre, T. J., Houwing, A. F. P., Palma, P. C., Rabbath, P. A. B., and Fax, J. S., "Optical and Pressure Measurements in Shock Tunnel Testing of a Model Scramjet Combustor," *Journal of Propulsion and Power*, Vol. 13, No. 3, 1997, pp. 388-394.

¹³Stalker, R. J., "Hypervelocity Aerodynamics with Chemical Non-equilibrium," *Annual Review of Fluid Mechanics*, Vol. 21, 1989, pp. 37-60.

¹⁴Anderson, G., Kumar, A., and Erdos, J., "Progress in Hypersonic Com-

bustion Technology with Computation and Experiment," AIAA Paper 90-5254, Oct. 1990.

¹⁵Anderson, G. Y., "Hypersonic Combustion-Status and Directions," *Combustion in High-Speed Flows*, edited by J. D. Buckmaster, T. L. Jackson, and A. Kumar, Kluwer Academic Publisher, 1994, pp. 19-51.

¹⁶Erdos, J. I., "Bridge from Hypersonic Aeropropulsion Ground Test Data to Flight Performance," AIAA Paper 98-2494, June 1998.

¹⁷Bakos, R. J., Morgan, R. G., and Tamagno, J., "Effects of Oxygen Dissociation on Hypervelocity Combustion Experiments," AIAA Paper 92-3964, July 1992.

¹⁸Anderson, R. C., Trucco, R. E., Rubin, L. F., and Swain, D. M., "Visualization of Hydrogen Injection in a Scramjet by Simultaneous PLIF and Laser Holographic Imaging," *Proceedings of the 1992 NASA Langley Measurement Technology Conferences*, NASA CP 3161, 1992.

¹⁹Rogers, R. C., Weidner, E. H., and Bittner, R. D., "Quantification of Scramjet Mixing in the Hypervelocity Flow of a Pulse Facility," AIAA Paper 94-2518, June 1994.

²⁰Ben-Yakar, A., and Hanson, R. K., "Experimental Investigation of Flame-Holding Capability of a Transverse Hydrogen Jet in Supersonic Cross-Flow," *Twenty-Seventh International Symposium on Combustion*, Combustion Inst., Pittsburgh, PA, 1998, pp. 2173-2180.

²¹Ben-Yakar, A., and Hanson, R. K., "Ultra-Fast-Framing Schlieren System for Studies of the Time Evolution of Jets in Supersonic Crossflows," *Experiments and Fluids* (to be published).

²²Ben-Yakar, A., "Experimental Investigation of Mixing and Ignition of Transverse Jets in Supersonic Crossflows," Ph.D. Dissertation, Dept. of Mechanical Engineering, Stanford Univ., Stanford, CA, Dec. 2000.

²³Heiser, W. H., and Pratt, D. T., *Hypersonic Airbreathing Propulsion*, AIAA Education Series, AIAA, Washington, DC, 1994.

²⁴Mirels, H., "Flow Nonuniformity in Shock Tubes Operating at Maximum Test Times," *Physics of Fluids*, Vol. 9, No. 10, 1966, pp. 1907-1912.

²⁵Mirels, H., "Test Time in Low Pressure Shock Tubes," *Physics of Fluids*, Vol. 6, No. 9, 1963, pp. 1202-1214.

²⁶Rogers, R. C., and Weidner, E. H., "Scramjet Fuel-Air Mixing Establishment in a Pulse Facility," *Journal of Propulsion and Power*, Vol. 9, No. 1, 1993, pp. 127-133.

²⁷Jacobs, P. A., Rogers, R. C., Weidner, E. H., and Bittner, R. D., "Flow Establishment in a Generic Scramjet Combustor," *Journal of Propulsion and Power*, Vol. 8, No. 4, 1992, pp. 890-899.

²⁸Davies, W. R., and Bernstein, L., "Heat Transfer and Transition to Turbulence in the Shock-Induced Boundary Layer on a Semi-Infinite Flat Plate," *Journal of Fluid Mechanics*, Vol. 36, No. 1, 1969, pp. 87-112.

²⁹Holden, M. S., "Establishment Time of Laminar Separated Flows," *AIAA Journal*, Vol. 9, No. 11, 1971, pp. 2296-2298.